Experimental Cell Research 351 (2017) 91–99

Contents lists available at ScienceDirect

Experimental Cell Research

journal homepage: www.elsevier.com/locate/yexcr

Neutrophil adhesion and crawling dynamics on liver sinusoidal endothelial cells under shear flow

Hao Yang[a,b], Ning Li[a,b], Yu Du[a,b], Chunfang Tong[a,b], Shouqin Lü[a,b], Jinrong Hu[a,b], Yan Zhang[a,b], Mian Long[a,b,*]

[a] Center of Biomechanics and Bioengineering, Key Laboratory of Microgravity (National Microgravity Laboratory), and Beijing Key Laboratory of Engineered Construction and Mechanobiology, Institute of Mechanics, Chinese Academy of Sciences, Beijing 100190, China
[b] School of Engineering Sciences, University of Chinese Academy of Sciences, Beijing 100049, China

ARTICLE INFO

Keywords:
Neutrophils
Liver sinusoids
Shear flow
Adhesive molecules
Kupffer cells

ABSTRACT

Neutrophil (polymorphonuclear leukocyte, PMN) recruitment in the liver sinusoid takes place in almost all liver diseases and contributes to pathogen clearance or tissue damage. While PMN rolling unlikely appears in liver sinusoids and Mac-1 or CD44 is assumed to play respective roles during *in vivo* local or systematic inflammatory stimulation, the regulating mechanisms of PMN adhesion and crawling dynamics are still unclear from those *in vivo* studies. Here we developed a two-dimensional *in vitro* sinusoidal model with primary liver sinusoidal endothelial cells (LSECs) and Kupffer cells (KCs) to investigate TNF-α-induced PMN recruitment under shear flow. Our data demonstrated that LFA-1 dominates the static or shear resistant adhesion of PMNs while Mac-1 decelerates PMN crawling on LSEC monolayer. Any one of LFA-1, Mac-1, and CD44 molecules is not able to work effectively for mediating PMN transmigration across LSEC monolayer. The presence of KCs only affects the randomness of PMN crawling. These findings further the understandings of PMN recruitment under shear flow in liver sinusoids.

1. Introduction

Liver is the largest organ with the functions of biosynthesis, metabolism, digestion, detoxification, and immunity. Various infectious or noninfectious factors such as hepatic virus, bacteria, parasite, alcohol intake, ischemia-reperfusion (I/R) and trauma can cause liver inflammation and damage. Almost in all kinds of liver diseases, neutrophils (polymorphonuclear leukocytes, PMNs) serve as an essential cell type for innate immune responses and PMN infiltration into hepatic tissue is widely observed to posses its function as a double-edged sword [1,2]. That is, PMNs can clear those infectious pathogens and damage tissue debris [3–5], whereas inappropriate accumulation of PMNs in liver microcirculation leads to severe tissue injury during drug-induced acute liver inflammation [6–8], I/R damage [9,10], alcohol liver disease [11,12], and other diseases. Thus, characterizing PMN recruitment in liver during hepatitis and liver injury are critical for understanding molecular mechanisms and potential clinical therapy.

PMN recruitment in liver mostly takes place in the capillary-like sinusoids rather than post-capillary venules which are the main locations for leukocyte infiltration in other tissues [13–15]. The liver sinusoid is a specialized capillary network with narrow luminal diameter (7–15 μm), slow blood flow (0.1–1 dyn/cm^2) [16–18], and is lined with fenestrated selectin-deficient liver sinusoid endothelial cells (LSECs) and liver resident macrophage Kupffer cells (KCs) [19]. All these features make the sinusoid a unique passage for flowing PMNs and affect their recruitment. Unlike the classical recruitment cascade which is initialed by selectin-mediated tethering and rolling, no rolling of PMNs is found in the inflammatory liver sinusoids, suggesting that selectins play null roles in PMN recruitment into sinusoids [20]. Since the absence of these traditional fast-kinetics adhesion molecules, it is hypothesized that PMN arrest occurs physically upon confined space and slow flow in the sinusoids [14,21,22]. In classical inflammatory cascade, LFA-1 and Mac-1, two β2 integrins expressed on PMNs, mediate PMN adhesion and crawling which are correlated to their respective molecular structures and distinct binding affinities [23,24]. However, the role of these adhesive molecules in the liver-specific PMN recruitment is diverse and not known clearly. On one hand, a body of evidences indicates that PMN migration in septic liver is independent on traditional adhesive molecules such as selectins, β2 integrins, intercellular adhesion molecule 1 (ICAM-1) and α4 integrins [13,14,18,20,22,25,26]. On the other hand, distinct adhesive molecules

* Corresponding author at: Institute of Mechanics, Chinese Academy of Sciences, Beijing 100190, China.
E-mail address: mlong@imech.ac.cn (M. Long).

http://dx.doi.org/10.1016/j.yexcr.2017.01.002
Received 4 December 2016; Received in revised form 5 January 2017; Accepted 7 January 2017
Available online 09 January 2017
0014-4827/

have unraveled liver-specific PMN recruitment under different inflammatory conditions. For example, Mac-1 dominates PMN recruitment in liver with local myxoma virus infection or fMLF stimulation, while the role of CD44-hyaluronan (HA) interactions is emerged with systemic LPS stimulation since Mac-1 expression is down-regulated by KC-secreted IL-10 [18,25,27]. Therefore, it is crucial to elucidate the respective contributions of those adhesive molecules in PMN recruitment in liver sinusoids under blood flow.

After being arrested on endothelial cells, PMNs need to crawl on the vessel wall to find proper emigration sites, cross the endothelium into the tissue, and finally execute their immune response functions. Although intraluminal crawling is a prerequisite for PMN transendothelial migration, the molecular mechanisms of PMN crawling have not been extensively investigated in contrast to those for cell adhesion and emigration processes. Only a few works indicate that Mac-1 and its endothelial ligands ICAM-1 and ICAM-2 are the major adhesive molecules involved in intraluminal crawling [28–30]. Specifically in liver sinusoids, PMN crawling percentage and velocity are down-regulated in ICAM-$1^{-/-}$ or Mac-$1^{-/-}$ mice during local fMLF stimulation or focal hepatic necrosis [25,31]. Understanding molecular mechanisms of PMN intraluminal crawling in the sinusoids is specially meaningful due to its featured biomechanical microenvironment of confined space and slow flow, which has been little known.

Here we applied a two-dimensional (2D) live-cell flow chamber assay to decipher the multistep process of PMN recruitment on LSEC monolayer under physiological flow [32]. Shear-resistant cell adhesion was quantified and flow-induced cell crawling was analyzed for fMLF-activated PMNs on TNF-α-stimulated LSECs. Related molecular regulations of LFA-1, Mac-1, and CD44 were determined. The presence of KCs in PMN recruitment in liver sinusoids were also discussed.

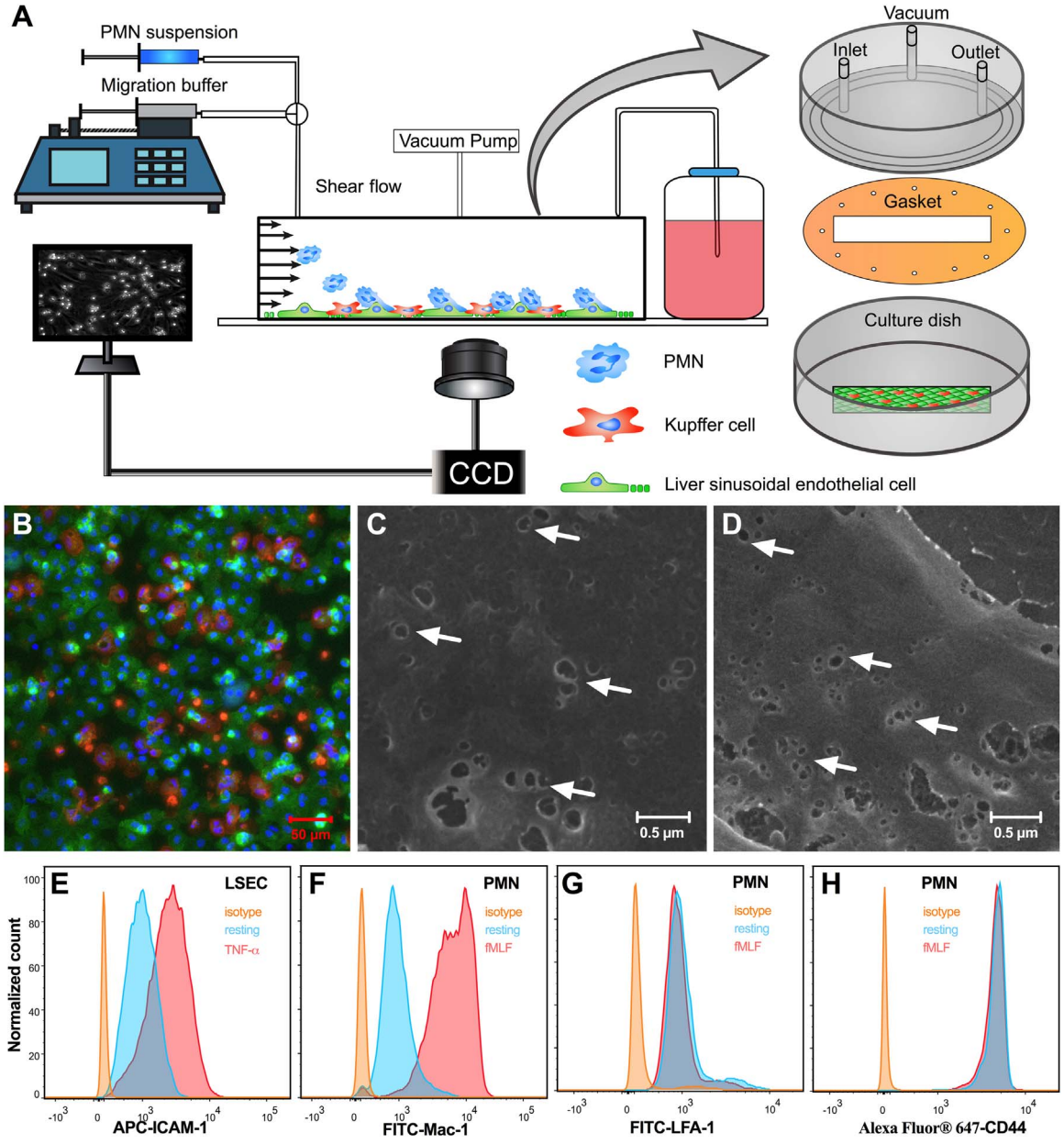

Fig. 1. Establishment of a 2D *in vitro* liver sinusoid model. (A) Schematic of the experimental system (not in scale). (B) Confocal images of murine LSECs (*green*; stained by FITC-conjugated anti-CD146 mAbs) cocultured with KCs (*red*; stained by PE-conjugated anti-F4/80 mAbs). Cell nuclei were stained by Hoechst 30332 (*blue*). (B-C) SEM images of LSECs cultured for 24 (C) and 72 h (D). *Arrows* indicate the fenestrae of cultured LSECs. (*E-H*) Flow cytometry analysis of ICAM-1s expressed on LSECs (E) and Mac-1s (F), LFA-1s (G) and CD44s (H) expressed on PMNs. Cells were incubated with respective fluorescein-conjugated primary mAbs or isotype-matched mAbs (control) in the absence or presence of TNF-α or fMLF stimulation.

2. Materials and methods

2.1. Ethics statement

All animal experiments were conducted in accordance with the guidelines of the Institutional Animal and Medicine Ethical Committee (IAMEC), and all the protocols were approved by the IAMEC at the Institute of Mechanics, Chinese Academy of Sciences.

2.2. Reagents

FITC-conjugated rat-anti-mouse CD11b (M1/70), FITC-conjugated rat-anti-mouse CD11a (M17/4), Alexa Fluor 647-conjugated rat-anti-mouse CD44 (1M7), APC-conjugated rat-anti-mouse ICAM-1 (YN1/1.7.4), as well as rat-anti-mouse blocking monoclonal antibodies (mAbs) against CD11a (M17/4) and CD11b (M1/70) were purchased from BioLegend (San Diego, CA). PE-conjugated human-anti-mouse F4/80 and FITC-conjugated rat-anti-mouse CD146 mAbs were from Miltenyi Biotec (Bergisch Gladbach, Germany). Rat-anti-human CD44 (Hermes-1) blocking mAbs were from Abcam (Cambridge, UK). Recombinant mouse TNF-α was from R & D (Minneapolis, MN), and bovine serum albumin (BSA) was from Bovogen (Melbourne, Australia).

2.3. Murine PMN isolation

PMNs were freshly isolated from the bone marrow of 8–12-week-old male C57BL/6 mice (Vital River Laboratories, Beijing, China). The bone marrow was flushed with Dulbecco's phosphate-buffered saline (DPBS) supplemented with 0.5% BSA and 2 mM EDTA from the femur and tibia. The single cell suspension was obtained by careful pipetting and filtration through 70-μm pore size nylon mesh cell strainer (BD Biosciences, Franklin Lakes, NJ). After centrifugation at 300×*g* for 10 min, the cell suspension was re-suspended for an equilibrium centrifugation using a Ficoll-Hypaque density gradient (Histopaque-1077 and Histopaque-1119, Sigma-Aldrich, St. Louis, MO) at 700×*g* for 30 min. PMNs were collected at the interface between the two layers, washed twice and then maintained in DPBS with 0.5% BSA at 4 °C before use.

2.4. Purification of murine LSECs and KCs

Primary LSECs and KCs were isolated from 8 to 12-week-old male C57BL/6 mice. Briefly, the liver from an anaesthetized mouse was perfused *via* the portal vein sequentially with balanced salt solution containing 5 mM glucose, 0.01% sodium heparin, and 5 mM EGTA and high glucose DMEM medium containing 4 mM $CaCl_2$, 2% FBS and 0.05% collagenase IV (Sigma-Aldrich, St. Louis, MO) at a flow rate of 5 ml/min for 5 min, respectively. Then the liver was harvested in high glucose DMEM medium and minced into small pieces. The undigested tissue fragments were removed by filtration through a cell strainer (200 μm). The cell suspension was centrifuged at 54×*g* for 3 min twice and the hepatocytes in the sediment were discarded in each centrifugation. The supernatant was finally collected and centrifuged at 500×*g* for 8 min. Those non-parenchymal cells (NPCs) in the pack were re-suspended with 3 ml of 24% Optiprep™ solution (Axis-Shield, Norway) in high glucose DMEM medium, followed by 3 ml 17.6%, 3 ml 11.7% and 2 ml 0% Optiprep™ solution in high glucose DMEM medium loaded on cell suspension carefully and orderly for density gradient equilibrium centrifugation at 1400×*g* for 18 min at 20 °C without brake. The cell suspension enriched with LSECs and KCs was collected from the interface of 17.6% and 11.7% Optiprep™ solution and washed by Hanks' balanced salt solution (HBSS) twice. Then the cell suspension stained with PE-conjugated anti-F4/80 and FITC-conjugated anti-CD146 mAbs in HBSS at 4°C in dark for 15 min was used for flow cytometry sorting by FACS Aria III (BD Biosciences), in which KCs were isolated by $CD146^-F4/80^+$ gating and LSECs were separated by $CD146^+F4/80^-$ gating. Collected LSECs were cultured alone or co-cultured with KCs in 35-mm culture dish with high glucose DMEM medium supplemented with 10% FBS, 100 U/ml penicillin, 100 μg/ml streptomycin and 1 mM L-glutamine at 37 °C with 5% CO_2.

2.5. Live-cell flow chamber assay

A circular GlycoTech flow cell system (Gaithersburg, MD) was used to test PMN adhesion, crawling, transmigration and shear resistance on LSECs alone or co-cultured with KCs (Fig. 1A). Shear flow was applied by a PHD22/2000 syringe pump (Harvard Apparatus, MA). Different shear stresses were acquired by setting corresponding volumetric flow rates and calculated from the following equation: $\tau=6\mu Q/h^2w$, where τ is the wall shear stress, μ is the medium viscosity at 20°C, Q is volumetric flow rate, and h and w are the channel height and width, respectively. Cultured cell monolayer or mixture was stimulated by 100 ng/ml TNF-α for 12 h and assembled into the flow cell system with a flow zone size of 20×5×0.254 mm. Immediately before the test, isolated PMNs were re-suspended in migration buffer (phenol red-free HBSS supplemented with Ca^{2+} and Mg^{2+} and 1% BSA) and stimulated with 1 μM fMLF at 37 °C and 5% CO_2 for 20 min. In some cases, fMLF-treated PMNs were pre-incubated with anti-Mac-1, anti-LFA-1 or anti-CD44 blocking mAbs. These resting or pretreated PMNs (2×10^6/ml) were then perfused over pre-formed LSEC monolayer and accumulated for 8 min at a shear stress of 0.1 dyne/cm^2. Then, the adhesion and crawling dynamics of PMNs on LSECs monolayer was recorded at 1 dyne/cm^2 at 20× objective by a CCD camera for 30 min. Images were taken from the video every 15 s and analyzed using the Manual Tracking Plugin interfaced with Image J software (National Institutes of Health, Bethesda, MD). Cell crawling parameters were calculated off-line from the acquired data using the Chemotaxis and Migration Tool 2.0 (IBIDI, Martinsried, Germany).

For testing shear-resistant PMN adhesion, the shear stress was increased stepwise from 1 to 2, 4, 8, 16, 32, 64 dyne/cm^2 for 30 s each. Remaining adherent PMNs on LSEC monolayer were recorded at 10× objective by a CCD camera and counted using Image J software. The normalized adhesion fraction was calculated by dividing the number of adherent PMNs at the endpoint of each shear phase by the number at the endpoint of 1 dyne/cm^2.

For defining the PMN transmigration dynamics, the time-lapse images were analyzed offline frame-by-frame every 5 s. Here a transmigrated PMN was determined by its color change from bright to black when it is transmigrating cross the monolayer. The time interval between the frame that the cell's color starts changing and the frame that the color has changed to be completely black was defined as the transmigration duration of this transmigrating cell. The numbers of transmigrated cells and total adherent cells were then counted and the percentage of PMN transmigration was calculated by dividing transmigrated cell number by total adherent cell number.

2.6. Confocal microscopy

LSECs co-cultured with KCs in dish were fixed with 4% paraformaldehyde in DPBS at room temperature for 15 min. After being washed 3 times with DPBS, the samples were blocked at 4 °C overnight in DPBS containing 1% BSA and then incubated with FITC-conjugated anti-CD146 mAbs for LSECs or PE-conjugated anti-F4/80 mAbs for KCs at 37 °C for 2 h. Washed samples were imaged using confocal laser-scanning microscopy (Zeiss LSM710, Germany).

2.7. Scanning electron microscopy

LSECs cultured at 24 h or 72 h were fixed with 2.5% glutaraldehyde in DPBS at room temperature for 2 h. After being rinsed 3 times with DPBS, the samples were dehydrated with ethanol gradient (50%, 70%,

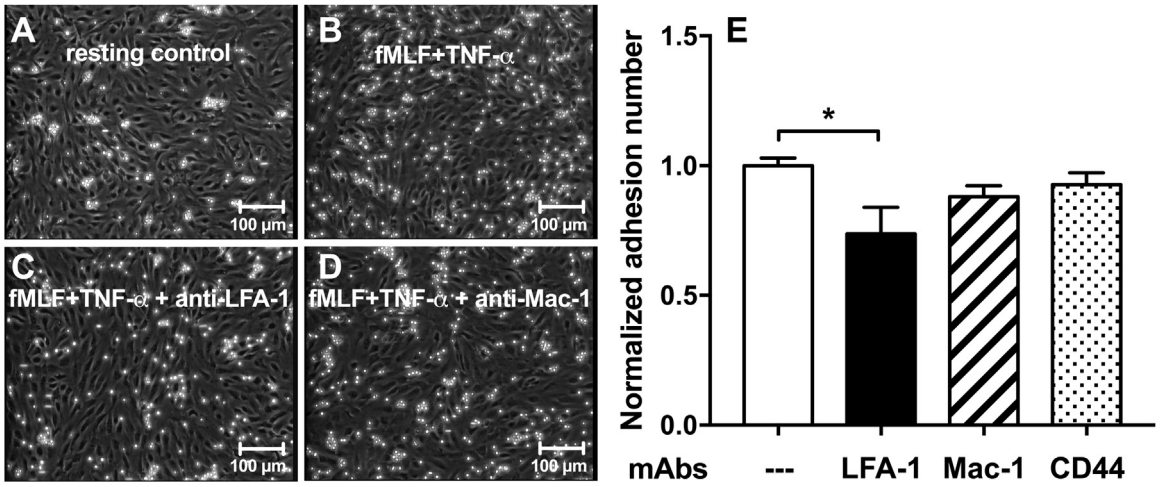

Fig. 2. Inflammatory stimulation increased PMN adhesion on LSECs under flow. Resting or fMLF-activated PMNs were perfused at shear stress of 0.1 dyne/cm^2 for 8 min to accumulate adhesion on resting or TNF-α stimulated LSECs. After being washed at 1 dyne/cm^2 for 1 min, the adhered PMNs were counted. (A-D) Optical images of PMN adhesion on LSEC monolayer for resting cells (A) or for those under fMLF and TNF-α stimuli alone (B) and with additional LFA-1 (C) or Mac-1 (D) blocking. Bar=100 μm. (E) fMLF-activated PMN adhesion numbers on TNF-α stimulated LSECs were normalized to average adherent cell number of resting control and plotted for the control and LFA-1-, Mac-1- or CD44-blocked PMNs. Data are presented as the mean ± SEM of 7 repeated runs from independent murine LSEC and PMN preparations. $^{*}p < 0.05$, $^{**}p < 0.001$ (one-way ANOVA followed by Newman-Keuls test).

80%, 90%, and 100%) for 10 min in each concentration. Collected samples were dried by a critical point dryer (Balzers CPD 030) and imaged by scanning electron microscope (KYKY-EM8000F, China).

2.8. Adhesive molecule expression

Expressions of LFA-1, Mac-1, and CD44 on PMNs and of ICAM-1 on LSECs were tested *via* flow cytometry (BD FACSCanto™ II, San Jose, CA). PMN suspension was incubated with 10 μg/ml of FITC-conjugated anti-mouse CD11b (M1/70), 10 μg/ml of FITC-conjugated anti-mouse CD11a (M17/4), or 2.5 μg/ml of Alexa Fluor 647-conjugated anti-mouse CD44 (1M7) mAbs at 4°C for 45 min. Cultured LSECs were digested with trypsin and incubated with 10 μg/ml of APC-conjugated anti-mouse CD54 mAbs. In some cases, PMNs were activated with 1 μM of fMLP for 20 min and LSECs were stimulated with 100 ng/ml of TNF-α for 12 h before test. Corresponding isotype-match antibodies were used as control.

2.9. Statistical analysis

Student's *t*-test or Mann-Whitney test was performed, depending on whether the data pass the normality test for two-group comparison. One-way ANOVA test followed by Newman-Keuls test was used for multiple-group comparison, while non-parametric Kruskal-Wallis test followed by Dunn's test was applied when the data cannot pass the normality test. Two-way ANOVA test followed by Newman-Keuls test was conducted for comparing the effects between adhesion molecule blocking groups and over multiple shear stress phases. multiple-group comparison with two parameters changed. *P* value was calculated using the corresponding statistical tests and considered statistically significant when $P < 0.05$.

3. Results

3.1. Establishment of a 2D in vitro liver sinusoid model

To test PMN recruitment under shear flow in liver microvasculature *in vitro*, we established a parallel flow chamber system containing a cell monolayer, a syringe pump and required valves to perfuse PMNs under shear flow, and a microscope with a CCD camera to visualize and record the interplay between PMNs and LSECs or LSECs co-cultured with KCs (Fig. 1A). Primary LSECs and KCs were isolated from C57BL/6 mice and cultured in a 35 mm culture dish. These cells were well identified by anti-CD146 mAb for LSECs and anti-F4/80 for KCs, respectively (Fig. 1B). Here LSECs tended to form an interconnecting monolayer and KCs were discretely distributed onto or in between LSECs. More importantly, numerous fenestrae were observed from SEM images on the surface of cultured LSECs, confirming their specific morphological features (Fig. 1C-D).

Sufficient expression of cell adhesive molecules is prerequisite to initiate the adhesion of PMNs to LSEC monolayer. To mimic those *in vivo* inflammatory stimuli, the LSEC monolayer was stimulated by 100 ng/ml TNF-α for 12 h and PMNs were stimulated by 1 mM fMLF for 20 min. It was found that ICAM-1 expression was significantly up-regulated by TNF-α stimulation (Fig. 1E). Mac-1 expression on PMNs was dramatically increased by fMLF stimulation, while LFA-1 and CD44 expressions were not affected (Fig. 1F-H). These results provided a working model of peripherical PMNs and resident hepatic cells from the same species for understanding flow-induced PMN adhesion and crawling.

3.2. Adhesion of PMNs on LSEC monolayer is LFA-1 dependent

We first tested PMN adhesion on LSEC monolayer by counting the accumulative number of adherent cells at a given shear stress. It was indicated that fMLF and TNF-α stimuli on respective PMNs and LSECs significantly enhanced PMN adhesion on LSEC monolayer compared with resting control (Fig. 2A-B), as expected. Since different cellular adhesive molecules on PMN surface are involved in PMN recruitment in the liver sinusoid under various pathological conditions [18,25,27,33], we further tested the dominance of those related molecules by blocking LFA-1, Mac-1, or CD44 respectively. Under inflammatory stimulation, PMN adhesion on LSEC monolayer was reduced significantly by LFA-1 blocking but remained unchanged by Mac-1 or CD44 blocking compared with resting PMNs (Fig. 2B-E). These findings suggest that LFA-1 plays an important role in PMN adhesion on LSEC monolayer while Mac-1 and CD44 have little effect, at least, in this 2D *in vitro* model.

In those pathological conditions such as liver fibrosis and cirrhosis, the patients may appear portal hypertension that result in a higher shear stress in the sinusoids. Thus, we applied a living-cell flow chamber system to test the dynamics of shear resistant PMN adhesion

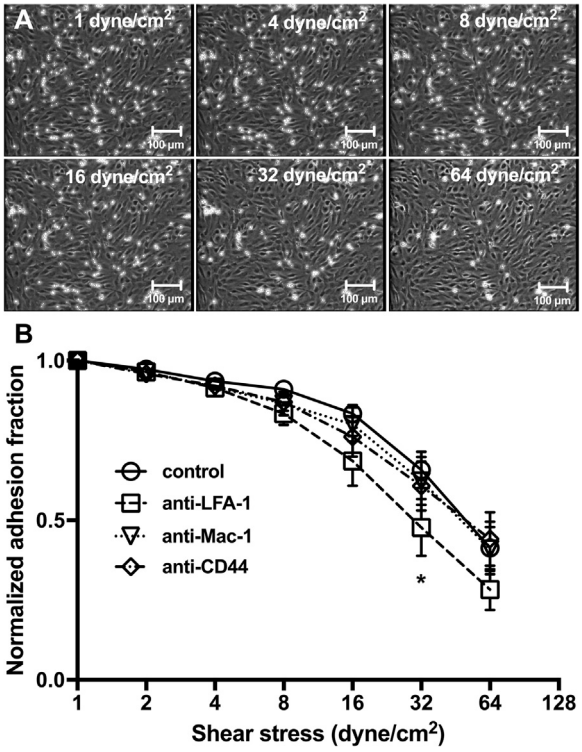

Fig. 3. Shear resistance of fMLF-activated PMNs on TNF-α-stimulated LSECs. After PMNs having adhered and crawled on LSECs at 1 dyne/cm^2 for 30 min, the stress was stepwise increased to 2, 4, 8, 16, 32, and 64 dyne/cm^2 for 30 s each to detach those adhered PMNs. (A) Optical images of fMLF-activated PMNs on TNF-α-stimulated LSEC monolayer at the endpoint of each phase. Bar=100 μm. (B) Normalized adhesion fraction was plotted for resting control and LFA-1-, Mac-1-, or CD44-blocked PMNs. Data are presented as the mean ± SEM of 7 repeated runs. $^*p < 0.05$ *versus* control at the same shear stress (two-way ANOVA followed by Newman-Keuls test).

on LSEC monolayer. Noting that the adherent cells were detached with the increased stress (Fig. 3A), majority of adhered cells (> 83 ± 3%) could resist the detachment at the shear stress of ≤16 dyne/cm^2, but a high fraction of adherent cells (> 35 ± 6%) were flushed away when the stress was lifted to 32 dyne/cm^2 or even larger (*cycles*; Fig. 3B). Blocking the adhesion molecules expressed on PMNs with anit-LFA-1 (*squares*), anti-Mac-1 (*triangles*) or anti-CD44 mAbs (*diamonds*) likely lowered the normalized adhesion fraction (Fig. 3B). Specifically, the fraction was comparable among the four groups when shear stress was relatively small (1–8 dyne/cm^2). The roles of adhesion molecules started to take effect when the stress was increased to 16 dyne/cm^2, where the fraction was reduced from 83 ± 3% in resting control to 69 ± 8% in LFA-1 blocking group. The significant role of LFA-1 was also verified by the lowest fraction at 32 dyne/cm^2 (65 ± 6%, 48 ± 9%, 62 ± 7% and 61 ± 8% for resting control, LFA-1, Mac-1 and CD44 blocking, respectively) and 64 dyne/cm^2 (41 ± 8%, 28 ± 6%, 41 ± 7% and 44 ± 8% for resting control, LFA-1, Mac-1 and CD44 blocking respectively). This result suggests that LFA-1 is dominant in resisting relatively high shear stress (16, 32 and 64 dyne/cm^2) than Mac-1 and CD44. This finding is also consistent with the observation that rupture force between LFA-1 and ICAM-1 on LSECs is larger than that for Mac-1 (unpublished data).

3.3. Mac-1 but not LFA-1 and CD44 limited flow induced PMN crawling on LSEC monolayer

Once being arrested on LSEC monolayer, PMNs start to crawl along the monolayer in the presence of blood flow. We next tested the role of β2 integrins and CD44 in post-arrest PMN crawling. Here sequential images for fMLF-activated PMNs and TNF-α-stimulated LSECs were collected every 15 s at 1 dyne/cm^2 and then analyzed by defining the various parameters of crawling dynamics (Fig. 4A). It was found that most arrested PMNs were able to crawl on the monolayer (supplemental video 1). Median crawling speed was significantly increased to 1.25-fold when blocking Mac-1 but not when blocking LFA-1 (0.90-fold) or CD44 (1.08-fold), as compared to that for resting control (Fig. 4B). Taking the mean velocity vector into consideration, Mac-1 blocking also up-regulated the median crawling velocity to 1.43-fold while LFA-1 (0.92 fold) and CD44 blocking (1.06-fold) did not show obvious effects (Fig. 4C). Thus, Mac-1s were dominant in decelerating either the scalar speed or the vectorial velocity of PMN crawling on LSEC monolayer. By contrast, LFA-1s and CD44s presented little effects in regulating PMN crawling speed.

Supplementary material related to this article can be found online at doi:10.1016/j.yexcr.2017.01.002.

Directionality is also crucial to represent PMN crawling dynamics on LSECs. We calculated the forward migration index (FMI) to *x*- (along with flow) or *y*-axis (perpendicular to flow) and the directness of crawling PMNs. The xFMI was significantly higher than zero (Fig. 4D) while the yFMI was fluctuating around zero (Fig. 4E), suggesting that PMNs intended to crawl along shear flow. Moreover, the xFMI (Fig. 4D) was slightly but significantly enhanced and the directness (Fig. 4F) was up-regulated when Mac-1s were blocked, implying that the existence of Mac-1s preferred to randomize PMN crawling along shear flow. By contrast, LFA-1 and CD44 were not strongly associated with crawling directionality since blocking these molecules showed little effects (Fig. 4D, F). These observations were supported by crawling trajectories of individual PMNs (Fig. 4G), where PMNs tended to crawl along flow direction with high fluctuation for resting control, LFA-1-, or CD44-blocked PMNs but with low fluctuation for Mac-1-blocked cells. Taken together, Mac-1s were found to brake PMN crawling and randomize PMN crawling on LSEC monolayer but LFA-1 and CD44 played little roles in PMN crawling.

3.4. PMN transmigration is independent on β2 integrin and CD44

Crawling PMNs are able to find the site for transmigrating cross LESC monolayer. As demonstrated in Fig. 5A, a fMLF-activated, adherent PMN usually takes about 0.4–27.4 min to reach the transmigrating site on TNF-α-stimulated LSEC monolayer in a flow-directed, curved trajectory. Although it is impossible to monitor the entire crawling duration of each transmigrating cell in a limited imaging window, we simply tested the crawling duration, the time interval from the starting point of imaging to the endpoint at the transmigrating site using an ensemble of crawling cells, in each case. It was indicated that the mean crawling duration was 13.3 ± 1.3, 11.2 ± 1.3, 12.1 ± 1.1, and 10.1 ± 1.1 min for resting control and those of LFA-1, Mac-1, and CD44-blocked PMNs, respectively (Fig. 5B). No statistical difference was found between any two of four groups, suggesting that any one of the three molecules is able to affect the crawling duration.

We also compared a key dynamic parameter of transmigrating duration, defined as the interval from the time point the cell arrives at the site to the endpoint it accomplishes the transmigration underneath LSEC monolayer. Again, the transmigration duration was not significantly affected when blocking LFA-1, Mac-1 or CD44 compared to control, yielding 2.4 ± 0.3, 2.1 ± 0.2, 1.9 ± 0.3, and 2.1 ± 0.2 min for resting control and those LFA-1- Mac-1-, and CD44-blocked PMNs, respectively (Fig. 5C). We also tested the ensemble features of PMN transmigration by comparing the fraction of transmigrated cells to total adherent cells. The percentage of cell transmigration was comparable for resting control (6.1 ± 1.6%) and for LFA-1- (5.6 ± 1.9%), Mac-1- (7.4 ± 2.0%), CD44-blocked (5.5 ± 2.4%) PMNs (Fig. 5D). These results suggest that PMN transmigration on our 2D liver sinusoid model is not able to be mediated by LFA-1, Mac-1 or CD44 alone.

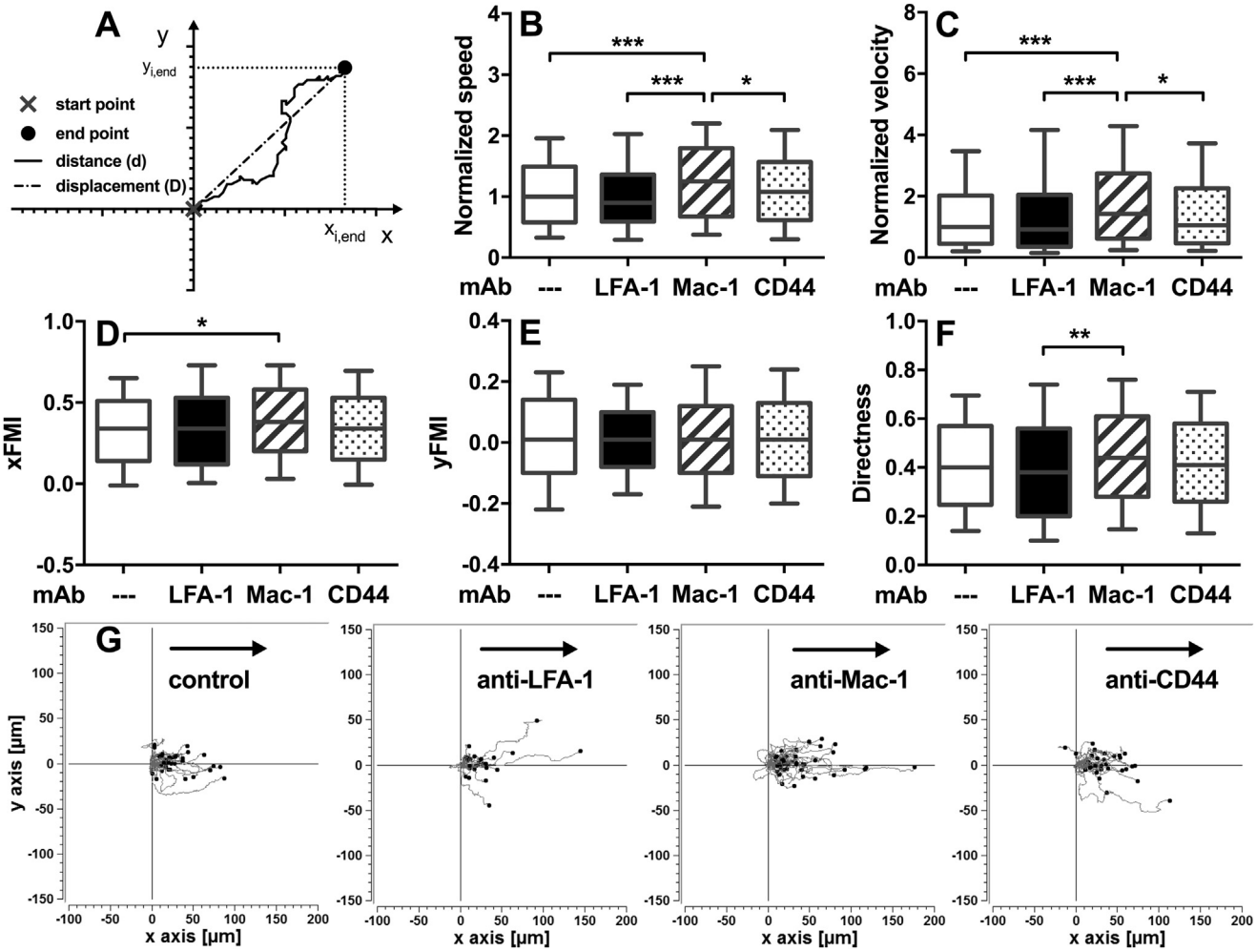

Fig. 4. Crawling dynamics of PMNs on LSEC under flow. Time courses of fMLF-activated PMNs crawling on TNF-α-stimulated LSECs at 1 dyne/cm^2 were recorded and analyzed using Manual Tracking Plugin interfaced with Image J software. (A) Schematic trajectory used for defining PMN crawling parameters. (B-F) Normalized crawling speed (=*d*/*time*) (B) and velocity (=*D*/*time*) (C) to the median of control, xFMI (=$x_{i,\ end}/D$) (D), yFMI (= $y_{i,\ end}/D$) (E) and directness (=*D*/*d*) (F) were plotted for control and LFA-1-, Mac-1-, or CD44-blocked PMNs. Data are presented, using a box-and-whiskers plot, as the median (*median line within box*) with the 25th and 75th percentiles (*upper and lower lines of box*), and the 10th and 90th percentiles (*whiskers above and below box*) of 343–444 cells in 6–7 repeated runs. (*G*) Typical trajectories of fMLF-activated PMNs crawling on TNF-α-stimulated LSEC monolayer. For each trajectory, the arrested sites of distinct PMNs were overlaid at the origin of the diagram (*x*/*y*=0/0) and the corresponding end points were indicated with *dots*. *Arrows* indicate the flow direction. $^{*}p < 0.05$, $^{**}p < 0.01$, $^{***}p < 0.001$ (Kruskal-Wallis test followed by Dunn's test).

3.5. PMN adhesion and crawling on LSECs alone or LSECs co-cultured with KCs were similar

In physiological condition, the liver sinusoid is mainly lined with LSECs and KCs. To define the role of KCs in PMN recruitment inside the sinusoids, we further compared PMN adhesion and crawling on LSECs alone or LSECs co-cultured with KCs. For this purpose, isolated LSECs and KCs were mixed and co-cultured at a physiological ratio of 2:1 and stimulated with 100 ng/ml of TNF-α for 12 h before exposing to shear flow. It was shown that the number of fMLF activated PMNs adhering on LSEC monolayer or LSEC-KC co-culture was comparable (Fig. 6A). PMN crawling speed, velocity and xFMI were slightly reduced without significant differences when KCs were presented on the monolayer (Fig. 6B-D). Similar with that on LSEC monolayer alone, xFMI of crawling PMNs on LSEC-KC monolayer was dramatically higher than zero while yFMI was equal to zero (Fig. 6D, E). Thus, co-culture of LSECs with KCs followed similar pattern of flow-directed cell crawling in a physiologically-mimicking cell composition. An exceptional case lied in significantly reduced median directness from 0.40 for LSECs alone to 0.35 for adding KCs in LSEC monolayer (Fig. 6F), implying that PMNs crawled more randomly on LSECs co-cultured with KCs than LSECs alone (supplemental video 1). To investigate which adhesion molecule induces such the effect, we compared the crawling directness between LSEC co-cultured with KCs and LSECs alone when blocking LFA-1, Mac-1 and CD44 respectively. The down-regulation of the directness in the presence of KCs disappeared in LFA-1 blocking group but remained unchanged in other three groups (Fig. 6F), implying that LFA-1s on PMN interacting with its ligands on KC might mediate the more random crawling on LSECs co-cultured with KCs. These results indicated that LSECs alone are sufficiently enough to undertake PMN adhesion and crawling in the liver sinusoid and the interplay between KCs and PMNs mediates highly randomized crawling to the flow direction.

4. Discussions

The recruitment of PMN is a core event during inflammation and cellular adhesive molecules play critical roles in PMN adhesion and crawling under blood flow. This process is specialized in the liver sinusoid due to its complexity of permeable blood flow and multi-typed cell composition. Here we set up a live-cell flow chamber system to investigate the dynamic features of PMN adhesion, crawling and transmigration under physiological flow on primary LSEC monolayer and adhesive molecules involved in these processes. This approach

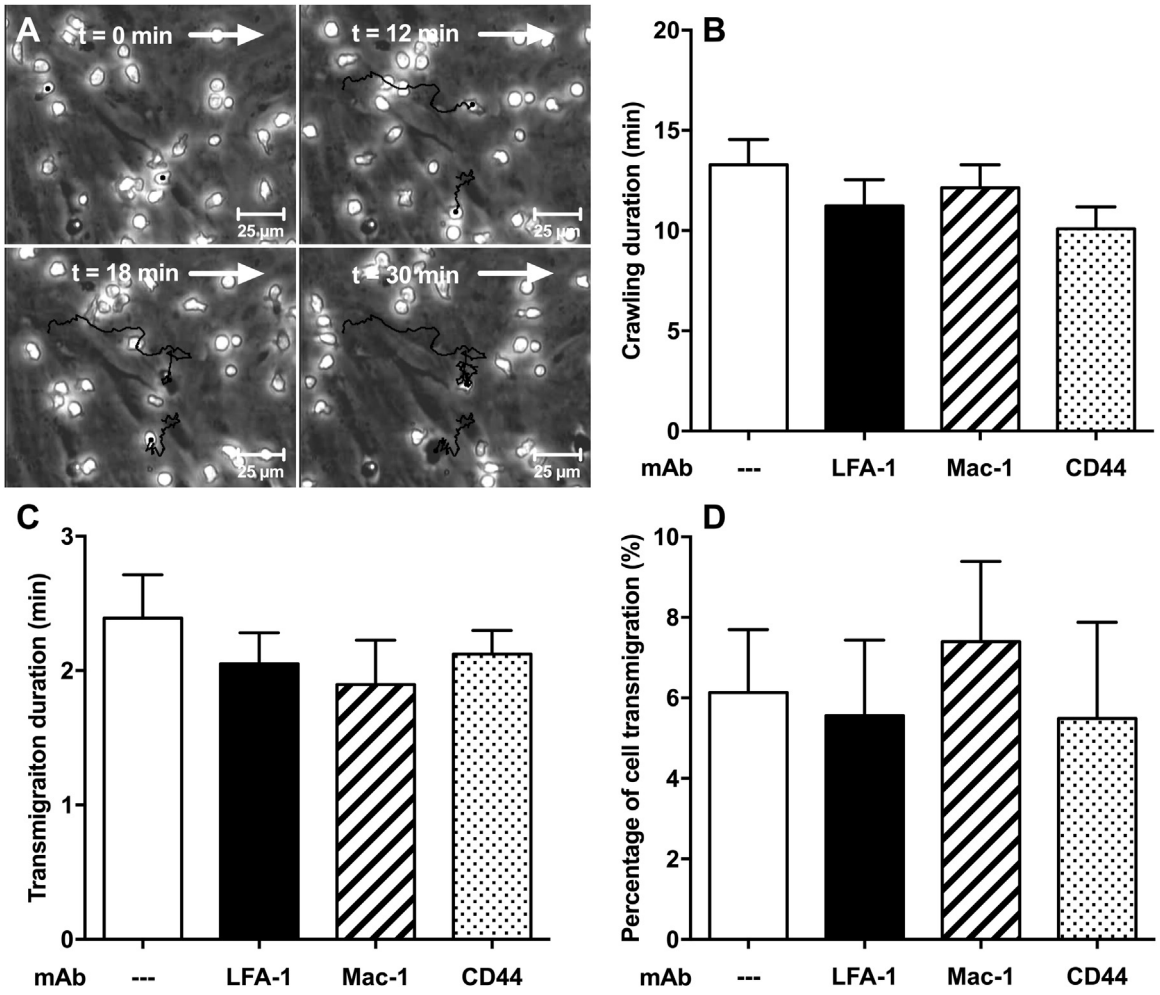

Fig. 5. Transmigration of fMLF-activated PMNs on TNF-α-stimulated LSECs under flow. (*A*) Optical images of fMLF-activated PMNs on TNF-α-stimulated LSEC monolayer at the time of 0, 12, 18, and 30 min at 1 dyne/cm^2. *Lines* and *dots* indicate typical trajectories of two PMNs before transmigrating underneath LSEC monolayer. *Arrows* indicate the flow direction. Bar=25 μm. (B-D) Cell crawling duration before transmigration (B), transmigration duration (C), and percentage of cell transmigration (D) were plotted for control and LFA-1-, Mac-1-, or CD44-blocked PMNs. Data are presented as the mean ± SEM of 28–38 cells in 6–7 repeated runs (B, C) or as the mean ± SEM of 6–7 repeated runs (D).

provides an *in vitro* platform to understand the biomechanics of PMNs interacting with hepatic cells in the sinusoids.

Methodologically, liver-specific *in vitro* microvascular model is difficult to establish. On one hand, isolated primary LSECs quickly lose their phenotype, as seen that rat LSECs cultured *in vitro* could maintain their fenestra phenotype within 3 days [34–36]. In our mouse LSEC model, the expression of LSEC marker CD146 (Fig. 1B) and the presence of their fenestration phenotype were maintained well within experimental duration (Fig. 1C-D), which makes this *in vitro* sinusoidal model workable, at least, in the functional tests reported here. On the other hand, classical multistep cascade of PMN recruitment is well studied using *in vitro* flow chamber assay and also verified by *in vivo* intravital microscopy on mesenteric and cremasteric microvasculature [37]. Recently, more and more tissue-specific evidences were obtained from *in vivo* intravital observations for such the organs as brain, liver, lung, and kidney, which has emerged new mechanisms of PMN recruitment different from the classical one [38,39]. Additionally, several *in vitro* flow tests were applied to elucidate the mechanisms of PMN recruitment on primary tissue-specific endothelial cells under shear flow or other mechanical or biochemical stimuli [28,32,40].

It has long been noticed that leukocytes tend to be physically trapped in liver sinusoids, mainly due to the comparable sizes between cell diameter and sinusoidal height. Thus the recruitment of PMNs in liver sinusoids is assumed to be independent on traditional adhesive molecules of E-selectin, P-selectin, β2 integrin, and α4 integrin [14,20,22]. These observations are recently challenged by the facts that leukocyte recruitment to the liver sinusoids is also related to different adhesive molecules including α4 integrin for Th1 cells, vascular adhesion protein 1 (VAP-1) for Th2 cells, β2 integrin for CD^{8+} T cells, and CD44 for monocytes [41–43]. Specifically, CD44 and HA interactions mediate PMN adhesion in liver sinusoids under LPS-induced inflammation while Mac-1, but not LFA-1, and ICAM-1 bindings dominate the adhesion during fMLF or myxoma virus-induced inflammation [18,25]. Intriguingly, our data indicated that LFA-1 dominates the adhesion at low shear stress of 1 dyne/cm^2 and also plays an important role in shear resistant adhesion at higher shear stress, while Mac-1 and CD44 display little roles in PMN adhesion (Figs. 2 and 3). This is not surprised since, unlike those *in vivo* conditions where the narrow luminal space of the sinusoid provides potential mechanical obstruction, the current *in vitro* model yielded a relatively unlimited space so that arrested PMNs need to resist the external shear stress through adhesive molecules. This interpretation is also supported by higher mechanical strength of LFA-1s than that Mac-1s when their counter-receptor of ICAM-1 is presented on LSEC surface (unpublished data), suggesting that LFA-1 could provide sufficient forces to resist the shear stress during PMN adhesion.

Following up the adhesion on endothelial cells, PMNs sequentially crawl on the luminal surface to the transmigration site. Mac-1 is thought to be the dominant molecule mediating PMN crawling since Mac-1 blocking reduces its crawling speed *in vivo* within liver sinusoids

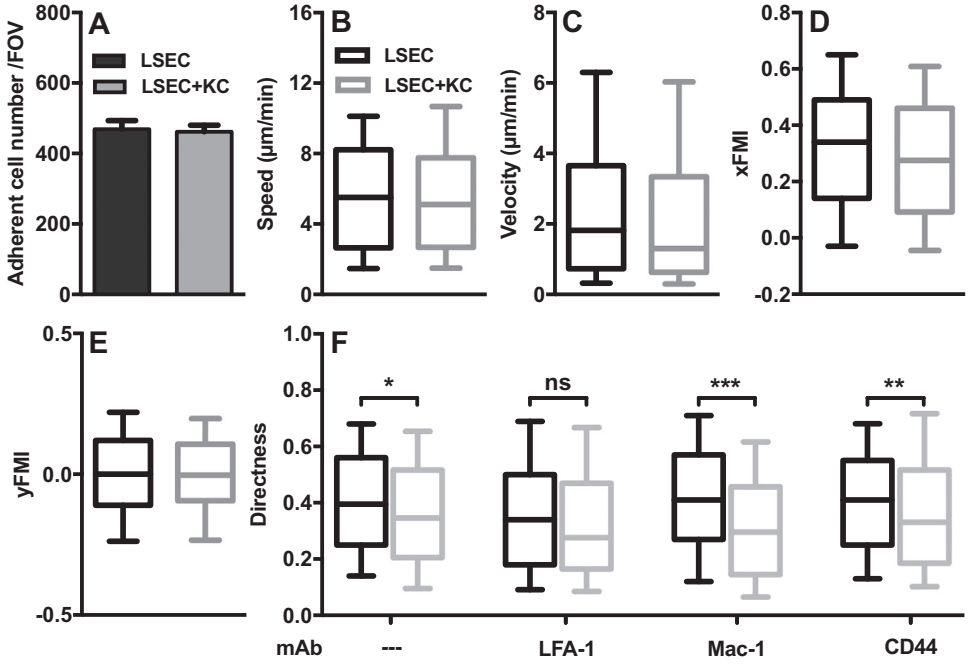

Fig. 6. Comparison of PMN adhesion and crawling on LSECs alone and co-cultured with KCs at 1 dyne/cm^2. Adhered cell number (A), crawling speed (B), velocity (C), xFMI (D), and yFMI (E) were plotted for fMLF-activated PMNs on TNF-α-simulated LSECs alone (*black bars*) or co-cultured with KCs (*grey bars*). Directness (F) under the same stimulus condition was plotted for control and LFA-1-, Mac-1-, and CD44-blocked PMNs. Data are presented as the mean ± SEM (A) or the median with 10–90 percentiles (*B-F*) of 366245–366 cells in 4 repeated runs. $^{*}p < 0.05$, $^{**}p < 0.01$, $^{***}p < 0.001$ for *t*-test (A) or Mann-Whitney-test (B-F).

and other microcirculation [25,30,31]. Here our results indicated that PMN crawling speed and velocity on LSECs were enhanced after Mac-1 blocking (Fig. 4B-C). Moreover, PMN crawling tended to align along flow direction by Mac-1 blocking (Fig. 4D-E), implying that the presence of Mac-1 randomizes the crawling directionality in liver sinusoids under shear flow. Generally, blood flow drives PMN movement inside microvasculature and β2 integrins on PMNs bind to their counter-receptors on endothelium for providing mechanical forces to resist PMN crawling along the flow. However, the roles of these adhesive molecules in PMN crawling are tissue-specific and highly depend on localized physiological structure and mechanical microenvironment. For example, PMN crawling velocity and the corresponding xFMI value on primary brain endothelial cells are enhanced when the adhesive molecules of β2 integrins, ICAM-1, and ICAM-2 are knocked out [28]. This is mainly because PMNs can flow and crawl over compact blood brain barrier without physical refinement and their mechanical resistance derived from bond forces of these molecular interactions can slow down PMN movement. By contrast, physical constriction of PMN movement in *in vivo* liver sinusoids or under *in vitro* static condition coordinates with these bond forces and then induces PMN crawling on LSEC monolayer at an appropriate velocity. Thus, our *in vitro* tests specify the respective roles of Mac-1 in crawling speed/velocity and directionality. Finally, PMNs transmigrate across LSEC monolayer to the inflamed liver tissue. In the current experimental set-up, PMN transmigration was not influenced by blocking β2 integrins or CD44 (Fig. 5), probably because one of the three receptors cannot function alone in transmigration [44].

It should be pointed out that PMN adhesion and crawling in *in vivo* liver sinusoids are much more complicated since multiple hepatic cells are presented inside the sinusoids under either quiescent or stimulated conditions. One example is to test potential roles of KC presence since KCs work cooperatively with LSECs to line up the sinusoids, which may also regulate PMN recruitment. Our data indicated that, at the given experimental setting, the mixed LSEC and KC monolayer has little effects on PMN recruitment except of more randomized crawling (Fig. 6). While elucidating the underlying signaling mechanisms is beyond the scope of the current work, one possible explanation is that extra KC numbers provide additional mechanical obstacle to the alignment of crawling PMNs under shear flow. Another example is to test the specificity of PMN recruitment on hepatic inflammatory cascade and understand the respective roles of these adhesive molecules using physiologically-mimicking stimulators. Our results demonstrated that TNF-α-induced primary LSECs can arrest large amount of fMLF-activated PMNs under physiological flow, in which LFA-1s provide major shear-resistance of PMNs adhesion while Mac-1 play roles in constraining crawling speed/velocity and directionality (Figs. 2–4). While further systematic studies are required to elucidate the roles of different cell composition under various cytokines or chemokines, these tests provided the cues to quantify PMN recruitment in liver sinusoids under physiologically-like microenvironment.

In conclusion, we investigated the dynamics of shear-induced PMN adhesion, crawling and transmigration on primary LSEC monolayer and the adhesive molecules involved. Our data indicated that LFA-1, but not Mac-1 and CD44, is positively dominant in static or shear-resistant PMN adhesion on LESCs. Mac-1, but not LFA-1 or CD44, is negatively dominant in PMN crawling velocity and directionality on LESCs. LFA-1, Mac-1, or CD44 has no effects in PMN transmigration presumably attributed to the incapability of any one of the three receptors alone. Moreover, KC presence only enhances randomized crawling but is not associated with cell adhesion and crawling dynamics. These results specify the functionality of respective receptors in liver sinusoids.

Disclosure

The authors declare no conflicts of interest, financial or otherwise.

Acknowledgements

This work was supported by National Natural Science Foundation of China (grant numbers 31230027, 91642203, 31661143044, 31110103918, and 31300776), and Frontier Science Key Project of and Strategic Priority Research Program of Chinese Academy of Sciences (grant numbers QYZDJ-SSW-JSC018 and XDB22040101).

References

[1] F. Heymann, F. Tacke, Immunology in the liver - from homeostasis to disease, Nat. Rev. Gastroenterol. Hepatol. 13 (2016) 88–110.

[2] A. Moles, L. Murphy, C.L. Wilson, J.B. Chakraborty, C. Fox, E.J. Park, J. Mann, F. Oakley, R. Howarth, J. Brain, S. Masson, M. Karin, E. Seki, D.A. Mann, A TLR2/S100A9/CXCL-2 signaling network is necessary for neutrophil recruitment in acute and chronic liver injury in the mouse, J. Hepatol. 60 (2014) 782–791.

[3] S.R. Clark, A.C. Ma, S.A. Tavener, B. McDonald, Z. Goodarzi, M.M. Kelly, K.D. Patel, S. Chakrabarti, E. McAvoy, G.D. Sinclair, E.M. Keys, E. Allen-Vercoe, R. DeVinney, C.J. Doig, F.H.Y. Green, P. Kubes, Platelet TLR4 activates neutrophil extracellular traps to ensnare bacteria in septic blood, Nat. Med. 13 (2007) 463–469.

[4] S.H. Gregory, E.J. Wing, Neutrophil-Kupffer cell interaction: a critical component of host defenses to systemic bacterial infections, J. Leukoc. Biol. 72 (2002) 239–248.

[5] C. Nathan, Neutrophils and immunity: challenges and opportunities, Nat. Rev. Immunol. 6 (2006) 173–182.

[6] P. Huebener, J.P. Pradere, C. Hernandez, G.Y. Gwak, J.M. Caviglia, X. Mu, J.D. Loike, R.E. Jenkins, D.J. Antoine, R.F. Schwabe, The HMGB1/RAGE axis triggers neutrophil-mediated injury amplification following necrosis, J. Clin. Investig. 125 (2015) 539–550.

[7] P.E. Marques, S.S. Amaral, D.A. Pires, L.L. Nogueira, F.M. Soriani, B.H. Lima, G.A. Lopes, R.C. Russo, T.V. Avila, J.G. Melgaco, A.G. Oliveira, M.A. Pinto, C.X. Lima, A.M. De Paula, D.C. Cara, M.F. Leite, M.M. Teixeira, G.B. Menezes, Chemokines and mitochondrial products activate neutrophils to amplify organ injury during mouse acute liver failure, Hepatology 56 (2012) 1971–1982.

[8] P.E. Marques, A.G. Oliveira, R.V. Pereira, B.A. David, L.F. Gomides, A.M. Saraiva, D.A. Pires, J.T. Novaes, D.O. Patricio, D. Cisalpino, Z. Menezes-Garcia, W.M. Leevy, S.E. Chapman, G. Mahecha, R.E. Marques, R. Guabiraba, V.P. Martins, D.G. Souza, D.S. Mansur, M.M. Teixeira, M.F. Leite, G.B. Menezes, Hepatic DNA deposition drives drug-induced liver injury and inflammation in mice, Hepatology 61 (2015) 348–360.

[9] M. Honda, T. Takeichi, K. Asonuma, K. Tanaka, M. Kusunoki, Y. Inomata, Intravital imaging of neutrophil recruitment in hepatic ischemia-reperfusion injury in mice, Transplantation 95 (2013) 551–558.

[10] A. Tsung, R. Sahai, H. Tanaka, A. Nakao, M.P. Fink, M.T. Lotze, H. Yang, J. Li, K.J. Tracey, D.A. Geller, T.R. Billiar, The nuclear factor HMGB1 mediates hepatic injury after murine liver ischemia-reperfusion, J. Exp. Med. 201 (2005) 1135–1143.

[11] A.P. Bautista, Chronic alcohol intoxication induces hepatic injury through enhanced macrophage inflammatory protein-2 production and intercellular adhesion molecule-1 expression in the liver, Hepatology 25 (1997) 335–342.

[12] A. Bertola, O. Park, B. Gao, Chronic plus binge ethanol feeding synergistically induces neutrophil infiltration and liver injury in mice: a critical role for E-selectin, Hepatology 58 (2013) 1814–1823.

[13] J. Carvalho-Tavares, A. Fox-Robichaud, P. Kubes, Assessment of the mechanism of juxtacrine activation and adhesion of leukocytes in liver microcirculation, Am. J. Physiol. Gastrointest. Liver Physiol. 276 (1999) G828–G834.

[14] A. Fox-Robichaud, P. Kubes, Molecular mechanisms of tumor necrosis factor alpha-stimulated leukocyte recruitment into the murine hepatic circulation, Hepatology 31 (2000) 1123–1127.

[15] W.-Y. Lee, P. Kubes, Leukocyte adhesion in the liver: distinct adhesion paradigm from other organs, J. Hepatol. 48 (2008) 504–512.

[16] A. Dash, M.B. Simmers, T.G. Deering, D.J. Berry, R.E. Feaver, N.E. Hastings, T.L. Pruett, E.L. LeCluyse, B.R. Blackman, B.R. Wamhoff, Hemodynamic flow improves rat hepatocyte morphology, function, and metabolic activity in vitro, Am. J. Physiol. Cell Physiol. 304 (2013) C1053–C1063.

[17] P.F. Lalor, D.H. Adams, Adhesion of lymphocytes to hepatic endothelium, Mol. Pathol. 52 (1999) 214–219.

[18] B. McDonald, E.F. McAvoy, F. Lam, V. Gill, C. de la Motte, R.C. Savani, P. Kubes, Interaction of CD44 and hyaluronan is the dominant mechanism for neutrophil sequestration in inflamed liver sinusoids, J. Exp. Med. 205 (2008) 915–927.

[19] B. Vollmar, M.D. Menger, The hepatic microcirculation: mechanistic contributions and therapeutic targets in liver injury and repair, Physiol. Rev. 89 (2009) 1269–1339.

[20] J. Wong, B. Johnston, S.S. Lee, D.C. Bullard, C.W. Smith, A.L. Beaudet, P. Kubes, A minimal role for selectins in the recruitment of leukocytes into the inflamed liver microvasculature, J. Clin. Investig. 99 (1997) 2782–2790.

[21] C.S. Bonder, M.N. Ajuebor, L.D. Zbytnuik, P. Kubes, M.G. Swain, Essential role for neutrophil recruitment to the liver in concanavalin A-induced hepatitis, J. Immunol. 172 (2004) 45–53.

[22] H. Jaeschke, A. Farhood, M.A. Fisher, C.W. Smith, Sequestration of neutrophils in the hepatic vasculature during endotoxemia is independent of beta2 integrins and intercellular adhesion molecule-1, Shock 6 (1996) 351–356.

[23] N. Li, S. Lu, Y. Zhang, M. Long, Mechanokinetics of receptor-ligand interactions in cell adhesion, Acta Mech. Sin. 31 (2015) 248–258.

[24] N. Li, D. Mao, S. Lu, C. Tong, Y. Zhang, M. Long, Distinct binding affinities of Mac-1 and LFA-1 in neutrophil activation, J. Immunol. 190 (2013) 4371–4381.

[25] G.B. Menezes, W.-Y. Lee, H. Zhou, C.C.M. Waterhouse, D.C. Cara, P. Kubes, Selective down-regulation of neutrophil Mac-1 in endotoxemic hepatic microcirculation via IL-10, J. Immunol. 183 (2009) 7557–7568.

[26] A.L. Patrick, J. Rullo, S. Beaudin, P. Liaw, A.E. Fox-Robichaud, Hepatic leukocyte recruitment in response to time-limited expression of TNF-alpha and IL-1beta, Am. J. Physiol. Gastrointest. Liver Physiol. 293 (2007) G663–G672.

[27] C.N. Jenne, C.H. Wong, F.J. Zemp, B. McDonald, M.M. Rahman, P.A. Forsyth, G. McFadden, P. Kubes, Neutrophils recruited to sites of infection protect from virus challenge by releasing neutrophil extracellular traps, Cell Host Microbe 13 (2013) 169–180.

[28] R. Gorina, R. Lyck, D. Vestweber, B. Engelhardt, Beta2 integrin-mediated crawling on endothelial ICAM-1 and ICAM-2 is a prerequisite for transcellular neutrophil diapedesis across the inflamed blood-brain barrier, J. Immunol. 192 (2014) 324–337.

[29] R. Lyck, G. Enzmann, The physiological roles of ICAM-1 and ICAM-2 in neutrophil migration into tissues, Curr. Opin. Hematol. 22 (2015) 53–59.

[30] M. Phillipson, B. Heit, P. Colarusso, L. Liu, C.M. Ballantyne, P. Kubes, Intraluminal crawling of neutrophils to emigration sites: a molecularly distinct process from adhesion in the recruitment cascade, J. Exp. Med. 203 (2006) 2569–2575.

[31] B. McDonald, K. Pittman, G.B. Menezes, S.A. Hirota, I. Slaba, C.C. Waterhouse, P.L. Beck, D.A. Muruve, P. Kubes, Intravascular danger signals guide neutrophils to sites of sterile inflammation, Science 330 (2010) 362–366.

[32] S. Shetty, C.J. Weston, D.H. Adams, P.F. Lalor, A flow adhesion assay to study leucocyte recruitment to human hepatic sinusoidal endothelium under conditions of shear stress, J. Vis. Exp. 85 (2014) e51130.

[33] B. McDonald, P. Kubes, Neutrophils and intravascular immunity in the liver during infection and sterile inflammation, Toxicol. Pathol. 40 (2012) 157–165.

[34] R.F. McGuire, D.M. Bissell, J. Boyles, F.J. Roll, Role of extracellular matrix in regulating fenestrations of sinusoidal endothelial cells isolated from normal rat liver, Hepatology 15 (1992) 989–997.

[35] T.L. Sellaro, A.K. Ravindra, D.B. Stolz, S.F. Badylak, Maintenance of hepatic sinusoidal endothelial cell phenotype in vitro using organ-specific extracellular matrix scaffolds, Tissue Eng. 13 (2007) 2301–2310.

[36] Y. Kim, P. Rajagopalan, 3D hepatic cultures simultaneously maintain primary hepatocyte and liver sinusoidal endothelial cell phenotypes, PLoS One 5 (2010) e15456.

[37] K. Ley, C. Laudanna, M.I. Cybulsky, S. Nourshargh, Getting to the site of inflammation: the leukocyte adhesion cascade updated, Nat. Rev. Immunol. 7 (2007) 678–689.

[38] J. Rossaint, A. Zarbock, Tissue-specific neutrophil recruitment into the lung, liver, and kidney, J. Innate Immun. 5 (2013) 348–357.

[39] E. Kolaczkowska, P. Kubes, Neutrophil recruitment and function in health and inflammation, Nat. Rev. Immunol. 13 (2013) 159–175.

[40] O. Steiner, C. Coisne, B. Engelhardt, R. Lyck, Comparison of immortalized bEnd5 and primary mouse brain microvascular endothelial cells as in vitro blood-brain barrier models for the study of T cell extravasation, J. Cereb. Blood Flow. Metab. 31 (2011) 315–327.

[41] C.S. Bonder, M.U. Norman, M.G. Swain, L.D. Zbytnuik, J. Yamanouchi, P. Santamaria, M. Ajuebor, M. Salmi, S. Jalkanen, P. Kubes, Rules of recruitment for Th1 and Th2 lymphocytes in inflamed liver: a role for alpha-4 integrin and vascular adhesion protein-1, Immunity 23 (2005) 153–163.

[42] B. John, I.N. Crispe, Passive and active mechanisms trap activated CD8+ T cells in the liver, J. Immunol. 172 (2004) 5222–5229.

[43] C. Shi, P. Velazquez, T.M. Hohl, I. Leiner, M.L. Dustin, E.G. Pamer, Monocyte trafficking to hepatic sites of bacterial infection is chemokine independent and directed by focal intercellular adhesion molecule-1 expression, J. Immunol. 184 (2010) 6266–6274.

[44] Y. Gong, Y. Zhang, S. Feng, X. Liu, S. Lü, M. Long, Dynamic contributions of P- and E-selectins to β2-integrin induced neutrophil transmigration, FASEB J. 31 (2017) 212–223.